Structural Network Topology Correlates of Microstructural Brain Dysmaturation in Term Infants with Congenital Heart Disease

Vincent J. Schmithorst, Ph.D.[1], **Jodie K. Votava-Smith, M.D.**[2], **Nhu Tran, Ph.D.**[2], **Richard Kim, M.D.**[3], **Vince Lee, B.S.**[1], **Rafael Ceschin, Ph.D.**[1,4], **Hollie Lai, M.D.**[5], **Jennifer A. Johnson, M.D.**[6], **Joan Sanchez De Toledo, M.D.**[7], **Stefan Blüml, Ph.D.**[5], **Lisa Paquette, M.D.**[8], and **Ashok Panigrahy, M.D.**[1,5]

[1.]Department of Pediatric Radiology, Children's Hospital of Pittsburgh of UPMC and University of Pittsburgh School of Medicine

[2.]Department of Pediatrics, Division of Cardiology, Children's Hospital Los Angeles, Los Angeles, CA

[3.]Division of Pediatric Cardiothoracic Surgery, Department of Surgery, Children's Hospital Los Angeles, Los Angeles, CA

[4.]Department of Biomedical Informatics, University of Pittsburgh, Pittsburgh, PA

[5.]Department of Radiology, Children's Hospital Los Angeles, Los Angeles, CA

[6.]Division of Pediatric Cardiology, Department of Pediatrics, University of Pittsburgh School of Medicine, Pittsburgh, PA.

[7.]Pediatric Cardiac Intensive Care Division, Department of Critical Care, University of Pittsburgh School of Medicine, Pittsburgh, PA

[8.]Department of Pediatrics, Division of Neonatology, Children's Hospital Los Angeles, Los Angeles, CA

Abstract

Neonates with complex congenital heart disease (CHD) demonstrate microstructural brain dysmaturation, but the relationship with structural network topology is unknown. We performed diffusion tensor imaging (DTI) in term neonates with CHD pre-operatively (N = 61) and post-operatively (N = 50) compared to healthy term controls (N = 91). We used network topology (graph) analyses incorporating different weighted and unweighted approaches and subject-specific white matter segmentation to investigate structural topology differences, as well as a voxel-based analysis (VBA) to confirm the presence of microstructural dysmaturation. We demonstrate cost-dependent network inefficiencies in neonatal CHD in the pre-operative and post-operative period compared to controls, related to microstructural differences. Controlling for cost, we show the presence of increased small-worldness (hierarchical fiber organization) in CHD infants pre-operatively, that persists in the post-operative period compared to controls, suggesting the early

Corresponding author: Ashok Panigrahy, MD, Department of Pediatric Radiology, Children's Hospital of Pittsburgh of UPMC, 45th Street and Penn Avenue, Pittsburgh PA 15201. panigrahya@upmc.edu, Phone: 412-692-5510, Fax: 412-692-6929.

presence of brain reorganization. Taken together, topological microstructural dysmaturation in CHD infants is accompanied by hierarchical fiber organization during a protracted critical period of early brain development. Our methodology also provides a pipeline for quantitation of network topology changes in neonates and infants with microstructural brain dysmaturation at risk for perinatal brain injury.

INTRODUCTION

Neurodevelopmental disabilities are the most common sequelae following surgical correction of different types of congenital heart disease (CHD) during infancy, with survivors increasingly reported to develop executive, attention, and social-emotional problems (Bellinger et al., 2011; Gaynor et al., 2015; Mussatto et al., 2015). Brain vulnerability in neonates with complex congenital heart disease (CHD) is multi-factorial and closely linked to metabolic disturbances *in utero*, secondary to aberrant hemodynamic/ oxygenation, genetic perturbations and possibly even placental factors (Limperopoulos et al., 2000; Sun et al., 2015). These metabolic disturbances may be related to altered WM microstructure in CHD infants reflected in diffusion tensor imaging (DTI) (Dimitropoulos et al., 2013; Li et al., 2014; Miller et al., 2007; Mulkey et al., 2014; Ortinau et al., 2012a; Paquette et al., 2013; Partridge et al., 2006). These DTI studies represent more "regional" correlates of microstructural brain dysmaturation, including tractography and manual region-of-interest [ROI], which may not reflect the true nature of global aberrant brain development in CHD infants, recently term "encephalopathy of congenital heart disease" (Gaynor, 2014; Volpe, 2014).

A "connectome" approach has the potential to delineate more "global" measures of brain dysmaturation when used in combination with DTI acquisition (Collin and van den Heuvel, 2013; Di Martino et al., 2014; Hagmann et al., 2012; Poldrack and Farah, 2015) as recently applied to pre-adolescent CHD subjects (Panigrahy et al., 2015) . The basis of "connectome" or network topology, includes the concept that cortical-based networks have optimized cost (number of connections) and metabolic trade-off architecture by maximizing topological properties and economic minimization of connection distance (Bullmore and Sporns, 2009; Bullmore and Sporns, 2012). The normal neonatal brain exhibits a "small-world" architecture, providing a balance between integration (global processing) and segregation (localized processing) (Cao et al., 2017; Huang et al., 2015; Song et al., 2017; Yap et al., 2011) which has the potential to be disrupted in infants with complex CHD. There are also a variety of graph metrics sensitive to hierarchical fiber organization, including centrality measures (Ball et al., 2014; van den Heuvel et al., 2012; van den Heuvel et al., 2014; van den Heuvel and Sporns, 2011; Zuo et al., 2012). Hierarchical brain fiber organization is thought to be genetically mediated (Chen et al., 2012; Fornito et al., 2011; Poldrack and Farah, 2015; Wedeen et al., 2012), which is highly relevant to understanding the genetic basis of poor neurodevelopment in patients with CHD.

Here, we combined network topology analysis with DTI to facilitate the characterization of more "global" measures of microstructural brain dysmaturation in term neonates with CHD compared to healthy term controls, leveraging an innovative non-biased quantitative

approach. First, we developed a novel method to parcel and mask the developing white matter, which controls for variations in FA values and heterogeneity of the microstructural elements of the un-myelinated white matter, known to be vulnerable in infants with complex CHD. Second, we also incorporated a neonatal specific white matter voxel-based analysis (VBA) pipeline to test the hypothesis that structural network topology differences are associated with microstructural dysmaturation changes (i.e. reduced fractional anisotropy and increased diffusivity) in selected neuroanatomic white matter tracts in our CHD infant population. Third, we quantitative the effects of using different weighted and unweighted approaches (FA/number of tracts/adjacency) and also controlling for cost on the structural network topology differences between CHD neonates/infants and controls to distinguish between WM microstructural and macrostructural changes, (Batalle et al., 2012; Brown et al., 2014). Our overall hypothesis is that we will detect altered DTI parameters (lower FA, increased MD/RD) due to microstructural WM changes in CHD neonates, which will also reflect in structural topology differences. We will also explore the possibility that CHD neonates will reflect macrostructural WM changes related to alterations in hierarchical fiber organization.

MATERIALS AND METHODS

Participants

The neonates in the study were recruited as part of a prospective observational study which was performed at two large medical centers, Children's Hospital Los Angeles (CHLA) and Children's Hospital of Pittsburgh of UPMC (CHP) from 2009–2015. The study was HIPAA compliant and approved by the Institutional Review Board at both institutions. The neonatal CHD cases were recruited from (1) pregnancies with fetal CHD confirmed with fetal echocardiography and (2) postnatally from admission to the cardiothoracic intensive care unit in the peri-operative period. Normal referents were recruited (1) from healthy pregnant volunteers and (2) postnatally from a normal newborn nursery. The inclusion criterion was critical CHD which was defined as a heart defect expected to require corrective or palliative cardiac surgery within the three months of life. Exclusion criteria for the CHD infants included congenital infection, preterm birth, genetic syndrome, documented chromosomal abnormalities and major congenital brain malformations. MRIs for CHD infants were obtained in either the preoperative (usually between 1- 7 days) or postoperative period (up to 13 weeks postnatally, but often sooner). The age range for healthy controls ranged between birth and thirteen weeks postnatally, encompassing the same range of the CHD infants.

Clinical Data

Medical records were reviewed for all participants and selected demographic variables were extracted including gestational age (GA) at birth and at the time of the scan. CHD lesion classification was performed by an experienced pediatric cardiologist (using pre- and post-natal echocardiogram data) and included: (1) single versus double ventricle cardiac anatomy; (2) obstruction to aortic outflow; (3) conotruncal abnormalities (abnormalities of great vessel septation and relationships), and (4) heterotaxy syndrome (abnormalities of viscero-atrial situs). These categories were not mutually exclusive. CHD patients were also separated into those with cyanotic versus acyanotic lesions. Cyanotic lesions included CHD

lesions that were characterized by postnatal mixing of pulmonary venous and systemic venous blood resulting in reduced oxygen saturation. CHD lesions such as transposition of the great arteries (TGA), single ventricles, tetralogy of Fallot (TOF), and total anomalous pulmonary venous return (TAPVR) were considered cyanotic types of CHD lesions. Coarctation or isolated shunt lesions were considered acyanotic types of CHD lesions.

Description of Cohorts

DTI data was acquired from 272 total prospectively recruited participants (both healthy term controls and term CHD). Data was rejected from 14 participants due to technical issues with the DTI acquisition (insufficient slice coverage for 4 participants; an unacceptably large (> 12 mm^3) voxel size for 10 participants). Data was rejected from 40 participants due to any form of brain injury or major brain dysgenesis (agenesis/dysgenesis of the corpus callosum for 7 participants; focal infarcts for 16 participants; punctate white matter lesions for 17 participants). Data was rejected from 11 participants due to unacceptable motion and/or slice dropout artifacts during the acquisition. Of note, our rejection rate due to motion was low since the neonates were scanned during natural sleep, the DTI acquisition was the first scan acquired after the localizer, and was repeated if motion was detected since these were research scans and sufficient time on the scanner was allocated. Data was rejected from 5 participants due to failure of the automated white matter segmentation algorithm. Thus, data was available from 202 participants, including 91 healthy controls, 61 CHD neonates scanned pre-operatively, and 50 CHD neonates scanned post-operatively. Demographic information for all participations is included in Table 1. Of note, the age at scan of the healthy controls spans a sufficient range to overlap both the pre-operative and post-operative CHD cohorts (which are similar in age). Clinical characteristics of the CHD participants are included in Table 2. The pre-operative incidence of punctate white matter injury was 10%, while the post-operative incidence of punctate white matter injury was 11%, relatively lower compared to other centers (Beca et al., 2013). These studies with punctate white matter injury were excluded from the analysis.

MR Acquisition

At both sites, a 3T scanner was used for all studies; scans were acquired on a Phillips Achieva at CHLA and Siemens Skyra or GE Excite at CHP. 2D EPI-DTI with 42 directions, TE/TR= 92 ms/12600 ms, b = 1000 s/mm^2, 2 mm slice thickness were acquired; in-plane resolution was close to 2 mm but varied slightly for some participants. Newborns were positioned in the coil to minimize head tilting. Newborns were fitted with earplugs (Quiet Earplugs; Sperian Hearing Protection, San Diego, CA) and neonatal ear muffs (MiniMuffs; Natus, San Carlos, CA). An MR-compatible vital signs monitoring system (Veris, MEDRAD, Inc. Indianola, PA) was used to monitor neonatal vital signs. All scans were performed using a multi-channel head coil. Preoperative research brain imaging was conducted when cardiothoracic intensive care unit (CTICU)/cardiology team determined the patient was stable for transport to the MRI scanner. The postoperative research scan was performed at less than thirteen weeks postnatal age either as an inpatient or outpatient. Most of the scans were research indicated and, as such, no additional sedation/anesthesia was given for purpose of the scan. Volumetric 3D T1 and T2 imaging and a blood sensitive sequence (GRE or SWI) were performed to evaluate for punctate white matter injury and to

evaluate for other major forms of brain injury (infarcts and hemorrhage) and congenital brain malformations. The fractional anisotropy (FA) map constructed from the DTI scan was used to evaluate for the presence of corpus callosum dysgenesis or agenesis.

Data analysis

Analyses were performed using in-house routines in IDL (ENVI, Boulder, CO); and routines in SPM8 (Wellcome Dept. of Cognitive Neurology, London, UK), FSL (fMRIB, Oxford, UK), and Brain Connectivity Toolbox (BCT; Indiana University, Bloomington, IN). A schematic of the graph analysis pipeline is presented in Figure 1.

Pre-processing and Generation of FA-independent Developing White Matter Segmentation

Data that was artificially upsampled during reconstruction by a factor of 2 (this was the case for some scans acquired on the GE scanner) was corrected by rebinning the data in the in-plane directions by a factor of 2. Frames with slice drop-out artifacts were removed using an automated routine in IDL. Motion and eddy current artifacts were corrected using routines in FSL, and maps of FA, λ_1, λ_2, λ_3, and direction of principal eigenvector computed. The λ_1 maps were normalized to the neonatal anatomical template (Shi et al., 2011) using routines in SPM8. The FA maps were then transformed to standard space using that transformation (resampled to 2 mm isotropic resolution). A study-specific FA template was constructed via averaging of all FA maps. The template was back-transformed into native space for each participant (using routines in SPM8 and the individual FA map as the reference) and the neonatal cortical parcellation atlas (Shi et al., 2011) was also transformed into native space using that transformation.

In addition, for each participant, to control for FA variation in the developing white matter, a white matter segmentation was performed using the FA map, the neonatal white matter, gray matter, and CSF templates (Shi et al., 2011) and the spm_preproc8 routine in SPM8. This procedure creates a white matter probability map from the FA image which is not dependent on the absolute values of FA in white matter (which vary across the population due to post-conceptional age, CHD status, and other factors; and regionally due to differing myelination status). The WM probability map (and not the FA, as is typically done) was used for the deterministic tractography.

Tractography and Construction of Unweighted and Weighted Graph Matrices

Deterministic tractography in native space was carried out using routines in IDL. Streamlines were constructed starting from each voxel with WM probability > 0.78 and were continued in both directions with stopping criteria of turning angle > 45 degrees or WM probability < 0.78 (using the white matter template). This threshold was determined via visual inspection to optimize the tradeoff between ensuring all streamlines remain in white matter and ensuring streamlines do not end prematurely due to a misclassified voxel. Secondary analyses showed that variation of this parameter did not appreciably affect cost and global efficiency (details in Appendix). Using the parcellation atlas (transformed into native space) to identify the cortical regions at both ends of each streamline we generated three 90×90 matrices using two different weighted matrices and one unweighted matrix). One of the two weighted approaches was termed "average FA" (each non-diagonal element

contains the FA averaged over all streamlines connecting two regions, and the other weighted approach was termed "number of tracts" (each non-diagonal element contains the total number of streamlines connecting the two regions). The unweighted approach was termed "adjacency" (each non-diagonal element is either 0 or 1, depending on whether at least one tract connects the corresponding cortical regions). We interpreted these difference in weighting as follows: "microstructural" changes reflect more in mean FA weighting while "macrostructural" change reflects more the other weighted approach "number of tracts" and the unweighted approach "adjacency". Of note, the "number of tracts" approach likely also weights towards total white matter volume.

Graph Analysis

Unweighted (for adjacency matrices) and weighted (for number of tracts and average FA matrices) metrics were computed using routines in the C++ version of BCT and in-house routines in IDL. The unweighted version of these routines was used for the adjacency matrices, while the weighted version was used for the number of tracts and the average FA matrices. Global metrics computed included cost (number of connections), global efficiency, transitivity, modularity, and small-worldness. Nodal metrics (which have a value for each of the 90 nodes) computed included clustering coefficient, nodal efficiency, eigenvector centrality, and participation coefficient (adjacency matrices only). As the modularity and small-world calculations depend on a stepwise optimization from a random starting point, 100 iterations were used and the results were averaged (small-world) or maximum value was used (modularity). Additionally, we examined our nodal level results in context of the developing brain network topology in the last trimester and early infancy (Alcauter et al., 2015; Gao et al., 2014; Gao et al., 2011; Gao et al., 2013; Menon, 2011; Thomason et al., 2014; Thomason et al., 2015).

Statistical Analysis for Network Topology

Our primary analysis was comparison of network topology measurements between CHD infants and healthy controls at two separate time points (pre-operative and post-operative) using separate GLM analyses. For these analyses, CHD was the variable of interest; while sex, post-conceptional age (PCA) at birth, PCA at scan, voxel size, and square root of the number of retained frames were included as covariates. Differences in scanner platform were handled as follows. Analysis was performed separately for each scanner in order to estimate the error variance (which may differ across platforms). Data was recombined including 2 additional dummy variables as covariates (each variable was coded 0 unless the scan was obtained on the Philips or GE scanner, respectively), and the GLM repeated given the error variances from each scanner. (This approach treats the effect of scanner as a fixed effect.) To assess statistical significance of tests which were applied to nodal graph metrics, the *IBHLog* version (Zeisel et al., 2011) (shown to be robust in cases of correlated dependent variables) of the FDR correction procedure (Benjamini and Hochberg, 2000) was used; results were deemed significant at $q < 0.05$. We repeated these analyses with cost included as a covariate, to investigate possible cost-independent differences in metrics.

Voxelwise Analyses for Anatomic Assessment of Microstructure

To confirm and delineate the neuroanatomic basis of microstructural brain dysmaturation in our CHD cohort, we compared DTI metrics including FA, mean diffusivity (MD), axial diffusivity (AD), and radial diffusivity (RD) on a voxelwise basis between CHD patients and controls. FA maps were normalized to the study-specific template using SPM8 and all maps (white matter probability, FA, λ_1, λ_2, λ_3) were normalized using that transformation; MD, AD, and RD were computed from the eigenvector maps. Only data points with a white matter probability > 0.78 were included in the analysis in order to prevent spurious results arising from misalignment of gray and white matter voxels; additionally, only specific voxels were included if data was available (e.g. the WM probability for that voxel was above threshold) from at least half of the participants. For each voxel, GLMs were performed in a similar manner as for the graph analysis metrics. A method (Ledberg et al., 1998) involving estimation of "noise maps" in order to estimate intrinsic spatial autocorrelation, was used to ascertain that a FWE-corrected p –value < 0.05 was obtained for an intensity threshold of Z > 2.5, a spatial extent threshold of 80 voxels (= 640 mm^3), and extrinsic Gaussian spatial filtering of $\sigma = 3$ mm (performed over included voxels only). This method of analysis was used in preference to the widely-used Tract-Based Spatial Statistics (TBSS) approach (Smith et al., 2006) as TBSS has been to shown to be vulnerable to spurious false positive results in the presence of brain morphological differences such as ventriculomegaly which are known to be present in CHD patients; while our white-matter masked voxelwise approach only suffers from loss of sensitivity (Schmithorst et al., 2013).

Secondary Analyses Relating DTI Parameters to Global Graph Metrics

We performed secondary analyses to investigate how microstructural DTI parameters are related to the global graph metrics we are computing: specifically, cost and global efficiency for each of the three connectomes. The above voxelwise analysis was repeated, except that the graph metrics instead of CHD status were used as the independent variable (CHD status being incorporate as a covariate).

Secondary Network Topology CHD Analyses

We also performed secondary analyses on the network topology metrics (not controlling for cost) incorporating the CHD cohort alone. First, we compared CHD neonates scanned post-operatively to those scanned pre-operatively to investigate a possible effect of operation. Next, since our cohort of CHD patients included majority male patients, consistent with a majority male prevalence of CHD in the population at large, we therefore tested for a significant effect of sex (including pre-operative/post-operative status as a covariate). Since our population is rather heterogenous with respect to type of heart lesion, we also tested for a significant effect for the three types of CHD (single vs. double ventricle, arch obstruction, and conotruncal) where sufficient sample size was available.

Additional Supplemental Analyses

To investigate the effect of changing the white matter threshold for the tractography, we repeated the tractography for WM thresholds of 70% and 86% and re-generated the global

graph analysis metrics (cost, global efficiency) for each connectome and computed Spearman correlation coefficients.

To investigate the possible effect of scanner on inter-subject variability, we calculated the inter-subject variability for each of the voxelwise DTI metrics, global graph theory metrics (cost and global efficiency), and a nodal graph theory metric (nodal efficiency). For the voxelwise metrics and for the nodal metric, the variance was averaged over all voxels or nodes used in the analysis. Additionally, we present data from an adult human phantom scanned on both the Siemens Skyra (CHP) and Philips Achieva (CHLA) scanner platforms. Correlations between voxelwise DTI metrics, and nodal graph metrics (nodal efficiency) are obtained. Since global efficiency is proportional to nodal efficiency averaged across all nodes, estimates for correlations of cost and global efficiency was also computed via bootstrap resampling (1000 samples with replacement).

RESULTS

Pre-operative Network Topology Differences between CHD and Term Healthy Control Neonates

We investigated differences in global network topology (Figure 2A, Table 3) in CHD neonates, pre-operatively, compared to healthy controls (Average FA connectome). CHD neonates demonstrated reduced cost and global efficiency (integration) in the pre-operative period, compared to healthy controls. There were no differences in transitivity (segregation), modularity (community structure) or small-worldness (balance of integration and segregation) in CHD neonates compared to healthy controls. We then investigated differences in nodal network topology (Figure 2B) in CHD neonates compared to healthy controls. At the nodal level, pre-operatively, there was diffuse reduced nodal efficiency in the CHD neonates compared to controls involving all lobes of the brain but no differences in any other nodal metrics including local efficiency and clustering coefficient (segregation), participation coefficient (segregation), and eigenvector centrality. Of note, greater differences in nodal efficiency were noted in the subcortical regions compared to the other cortical regions. Next, in order to delineate the microstructural anatomic basis of these differences in both global and nodal network topology, we applied a voxel-based analysis to the diffusion tensor data between CHD neonates and healthy controls (Figure 2C). Accordingly, agreeing with previous reports (Dimitropoulos et al., 2013; Li et al., 2014; Miller et al., 2007; Mulkey et al., 2014; Ortinau et al., 2012a; Paquette et al., 2013; Partridge et al., 2006), neonates with CHD pre-operatively compared to term controls showed increases in MD, RD and AD and decreases in FA in multiple white matter regions including subcortical white matter tracts, the genu and splenium of the corpus callosum (CC) (interhemispheric), and both the fronto-occipital fasciculus (FOF) and the inferior longitudinal fasciculus (ILF) (intrahemispheric), indicative of microstructural WM change which could include decreased fiber density or organization or changes in axonal caliber.

Post-operative Network Topology Differences between CHD and Term Healthy Control Neonates

We investigated differences in global network topology (Figure 3A, Table 3) in CHD infants, post-operatively, compared to healthy controls (Average FA connectome). CHD neonates again demonstrated reduced cost in the post-operative period, compared to healthy controls, but to a lesser degree compared to the pre-operative period. There were no differences in global efficiency, modularity (community structure) or small-worldness (balance of integration and segregation), although reduced segregation was found. We then investigated differences in nodal network topology (Figure 3B) in CHD infants compared to healthy controls. At the nodal level, post-operatively, there was again noted reduced nodal efficiency in the CHD neonates compared to controls in predominately frontal and parietal-occipital cortical regions, with these differences restricted to fewer regions compared to the pre-operative period. There were no differences in any other nodal metrics including local efficiency and clustering coefficient (segregation), participation coefficient (segregation), and eigenvector centrality. Next, in order to delineate the microstructural anatomic basis of these differences in both global and nodal network topology, we applied a voxel-based analysis to the diffusion tensor data between CHD neonates and healthy controls (Figure 3C). Similar to the preoperative scan, neonates with CHD post-operatively compared to term controls showed increases in MD, RD and AD and decreases in FA in multiple white matter regions including subcortical white matter tracts, the genu and splenium of the corpus callosum (CC) (interhemispheric), and both the fronto-occipital fasciculus (FOF) and the inferior longitudinal fasciculus (ILF) (intrahemispheric), indicative of microstructural changes which could include decreased fiber density and/or organization. Of note, the magnitude of reduced FA difference in the FOF and ILF was less in the post-operative period compared to the pre-operative period. Also, the magnitude of increased diffusivity difference was less in the post-operative period compared to the pre-operative period.

Effect of Connectome

We repeated the above analyses using the number of tracts and the adjacency connectomes. For CHD neonates scanned pre-operatively, reduced cost and global efficiency are still present (Figure 4A, 4E; Table 3) and reduced nodal efficiency is also seen (Figure 4B, 4F) although concentrated in posterior, subcortical, and frontal regions. For CHD neonates scanned post-operatively, no significant results are seen using the adjacency connectome (Figure 4G, 4H; Table 3). For the number of tracts connectome, cost and global efficiency are reduced, and again reduced nodal efficiency is concentrated in posterior and frontal regions (Figure 4C, 4D; Table 3).

Network Topology Differences between CHD and Term Healthy Control Neonates Controlling for Cost

After controlling for cost, increased small-worldness was seen both pre-operatively and post-operatively in the # tracts and average FA connectome (Figure 5, Table 4). (Small-worldness is a metric related to the balance between network integration and segregation.) Additionally, increased efficiency was seen post-operatively in the adjacency connectome. No significant differences were found for any of the nodal metrics. These results indicate a

reorganization of the brain structural topology at a macrostructural level unrelated to network cost.

Secondary Analyses Relating Graph Parameters to DTI Metrics

Significant associations were found throughout the white matter between DTI metrics (RD, MD, AD, FA) and cost/global efficiency for all three connectomes (Figure 6). The effect was more highly significant for the average FA connectome compared with the # tracts or adjacency connectomes, consistent with the average FA connectome being more highly weighted towards microstructural differences.

Secondary Network Topology CHD Analyses

We did not find any significant differences in network topology parameters between pre-operative and post-operative CHD patients for the adjacency and average FA connectomes. However, for the # of tracts connectome, we found significant increases in cost ($p < 0.05$), global efficiency ($p < 0.01$), and small-worldness ($p < 0.05$) in CHD neonates post-operatively compared to pre-operatively. Additionally, there were widespread regions (mainly frontally and sub-cortically) with increased nodal efficiency (data not shown).

We did not find any significant differences in network topology parameters between male and female CHD patients. Regarding type of lesion, no significant differences were found related to arch obstruction or single/double ventricle. The only difference found for conotruncal was reduced transitivity ($p < 0.05$) for the # of tracts connectome.

Additional Supplemental Analyses

The specific choice of white matter threshold for the tractography was not found to have a large effect on the graph metrics (cost/global efficiency), as even a (very liberal) threshold of 70% or a (very strict) threshold of 86% resulted in correlation coefficients of 0.97 or better (results in Appendix).

There was only a limited effect of scanner platform on between-subject variability for most metrics, with standard deviations within a factor of 1.5 of each other (results shown in Appendix). Results from the human phantom data show a large correlation for FA/AD and for nodal efficiency/global efficiency across platforms (Rs between 0.75 and 0.92). Less reliability is shown for MD/RD (Rs between 0.5 and 0.6). This is likely due to differences in geometric distortion and partial volume between the scanners, which will more strongly affect estimated diffusion parameters perpendicular to the axon direction as compared to parallel.

DISCUSSION

Neonates with CHD have been previously documented to have reduced FA, in the preoperative and postoperative period (Dimitropoulos et al., 2013; Li et al., 2014; Miller et al., 2007; Mulkey et al., 2014; Ortinau et al., 2012a; Paquette et al., 2013; Partridge et al., 2006). Here, we present a pipeline which demonstrates network inefficiencies present at birth in CHD neonates in the pre-operative and post-operative periods, providing topological

correlates of microstructural brain dysmaturation. These network inefficiencies were dependent on cost which is the metric related to metabolism or wiring of connections. Our VBA analysis confirmed that reduced FA and increased diffusivity also characterize these changes that agree with prior studies in CHD neonates (Dimitropoulos et al., 2013; Li et al., 2014; Miller et al., 2007; Mulkey et al., 2014; Ortinau et al., 2012a; Paquette et al., 2013; Partridge et al., 2006). Importantly, after controlling for cost, we found hierarchical organizational changes (i.e. small worlndess) also present at birth preoperatively which persist into the postoperative period in CHD neonates, suggesting that brain reorganization likely starts *in utero* and persists into the early postnatal period. These findings are concordant with regional alterations in cortical maturation which have also been delineated in complex CHD (Clouchoux et al., 2013; Licht et al., 2009; Ortinau et al., 2013). Delayed cortical maturation has been shown to be a better predictor of early neurodevelopmental outcome as compared to white matter injury scores (Beca et al., 2013).

Most structural network topology studies, up to this point, have been performed in healthy and preterm neonates (Ball G et al. 2014; van den Heuvel MP et al. 2014). As such, little is known about the effects of CHD on the structural network topology of the neonatal brain as found using graph analysis. The DTI graph metrics characterize how important or central a node is to the network and each seems to capture independent aspects of brain networks (Ball et al., 2014; Scheinost et al., 2015; van den Heuvel et al., 2012; van den Heuvel et al., 2014; van den Heuvel and Sporns, 2011; Watanabe and Rees, 2015; Zuo et al., 2012). Here, we show that reduced fractional anisotropy and increased radial diffusivity is associated with reduced metabolic wiring cost and network efficiency in neonates with CHD, predominately at birth in the pre-operative period. In parallel, we also delineated cost-controlled differences related to hierarchical fiber organization, as neonates with CHD operatively have increased small-worldness present in both the pre-operative and post-operative period. Small-worldness is a metric denoting balance between network integration and segregation. Importantly, our methodology, by applying a special template to the developing white matter which controls for the marked variation in FA in the central and peripheral matter, is not sensitive to spurious differences in topology resulting from typical tractography approaches which utilize a fixed FA threshold.

Cost-dependent differences in CHD and microstructure of cortical association fibers

CHD patients pre-operatively display reduced metabolic wiring cost for all three weighted/un-weighted approaches (adjacency, # of tracts, or mean FA), reflecting a robust global metric related to microstructural WM change. Reductions in global efficiency were also seen, since efficiency is highly correlated with cost. These differences suggest that the etiology for reduced metabolic wiring cost of the developing white matter in CHD is highly related to the fetal period. The epoch of fetal brain development in the CHD subjects most closely tied to metabolic derangement of wiring cost may be the last trimester, as reduced fetal brain volume and abnormalities of fetal brain neuronal-axonal metabolism (using MR spectroscopy) and fetal oxidative metabolism have been documented during the last trimester (Limperopoulos et al., 2000; Sun et al., 2015). In addition, diffuse and regional reduction in brain volume has been delineated pre-operatively in neonates with CHD (Ortinau et al., 2012a; Ortinau et al., 2012b; Owen et al., 2014; von Rhein et al., 2015) and

post-operatively in older CHD patients (von Rhein et al., 2014; Watanabe et al., 2009). Post-operatively, reductions in cost were still seen using the two weighted approaches, indicating these effects persist post-operatively to some extent. Accordingly, widespread decreases in nodal efficiency were seen both pre- and post-operatively but concentrated in occipito-parietal, subcortical, medial backbone, and prefrontal regions. Our results suggest a reduction of this effect post-operatively, also given the increased cost, global, efficiency, and nodal efficiency seen when post-operative CHD neonates are compared with pre-operative CHD. Of note, postnatal imaging of CHD neonates shows differential reduced volume of frontal and subcortical regions (Ortinau et al., 2012a; Owen et al., 2014; Watanabe et al., 2009). Some of the nodal regions showing efficiency reductions, particularly in the operculum region, overlap with known postnatal and fetal regional cortical alterations in patients with complex CHD (Clouchoux et al., 2013; Licht et al., 2009; Ortinau et al., 2013).

Our analysis also investigated the potential etiology of reduced metabolic wiring cost by measuring associated radial diffusivity (RD) and axial diffusivity (AD) changes and localizing the anatomic substrate of these microstructural alterations using a neonatal specific white matter VBA pipeline. We found that the changes in cost/global efficiency were driven by increased RD and increased AD, in neonates with CHD pre-operatively as well as post-operatively. Increased RD is likely indicative of decreased fiber density or organization, suggesting easier diffusion in the interstitial space perpendicular to the axonal direction. Decreased fiber density will also lead to increased AD, although the magnitude of the increase will depend on the amount of fiber tortuosity; the magnitude of the AD increase will be much less in regions with a more streamlined fiber organization (as there are few barriers to diffusion parallel to the axonal diffusion direction). Our results also show that increased RD is present in both cortical association fibers (both interhemispheric and intrahemispheric) and subcortical fibers. While interhemispheric connectivity has previously been demonstrated to be altered in neonates with CHD (Dimitropoulos et al., 2013; Li et al., 2014; Miller et al., 2007; Mulkey et al., 2014; Ortinau et al., 2012a; Paquette et al., 2013; Partridge et al., 2006), these studies did not investigate intrahemispheric connectivity, mostly owing to the use of more selected/regional interrogation of microstructural abnormalities. Our data clearly shows that the inferior longitudinal fasciculus (ILF) and the fronto-occipital fasciculus (FOF) demonstrate alterations in neonates with CHD. The ILF/FOF are critical pathways for ventral visual regulation and social-emotional functions, which are known to be abnormal in patients with complex CHD (Bellinger et al., 2015).

CHD and hierarchical fiber organization after controlling for cost

We delineated cost-independent differences by controlling for network cost in our analyses. This technique allowed us to investigate hierarchical fiber organization at the global level, as well as at the nodal level (Ball et al., 2014; Scheinost et al., 2015; van den Heuvel et al., 2012; van den Heuvel et al., 2014; van den Heuvel and Sporns, 2011; Watanabe and Rees, 2015; Zuo et al., 2012). We found that controlling for cost, CHD neonates pre- and post-operatively globally have increased small-worldness for the weighted approaches, supporting a large-scale hierarchical reorganization of structural topology, as small-worldness represents a balance between network segregation and integration; small-world networks have high segregation but similar integration as compared to a random graph.

Thus, structural brain connectivity in CHD may undergo reorganization post-operatively to maintain the brain's resilient structure (Fling et al., 2012; Fling et al., 2011; Langan et al., 2010). Interesting, we found these differences in small worldness present to a similar extent in the both the pre-operative period and the post-operative period, suggesting a protracted period of brain reorganization during a critical period of early postnatal brain development. Our DTI VBA results also support a hierarchical organization post-operatively, with higher MD in CHD neonates in most regions but reduced MD in the internal capsule, consistent with decreased interhemispheric but increased intrahemispheric connectivity.

Etiological considerations

The microstructural alterations seen in CHD neonates may be the effect of prenatal hypoxia-ischemia and its effect on the developing white matter *in utero*, particularly during the last trimester, as described above. As normoxia is restored via surgery, these alterations reverse trend to some extent, as seen in our data, though some of the CHD neonates remain hypoxemic after neonatal surgical palliation. This effect is likely mediated by pre- and peri-operative factors, as previous studies demonstrated that the type of surgical technique used for correction of the heart lesion seems to be relatively less important in driving poor neurodevelopment in the CHD population compared to innate patient factors (Hoffman et al., 2015; Newburger et al., 2012). Thus, there is likely still on-going postnatal vulnerability of the developing white matter in this population, a concept supported by other neurodevelopmental outcome studies in CHD neonates (Newburger JW et al. 2012).

We hypothesize, however, that fiber organization differences may have a genetic etiology as well, as seen in other neurological disorders (Chen et al., 2012; Fornito et al., 2011; Poldrack and Farah, 2015; Wedeen et al., 2012). Findings from a recent large-scale mouse forward genetic screen for mutations causing CHD suggest the possibility that heart lesion and poor neurodevelopmental outcomes may also share a common genetic etiology, as among the mutations recovered causing CHD are many genes known to play important roles in neurodevelopment including mutations in *Robo1* and *Semaphorin/PlexinD1*, genes encoding proteins regulating chemorepulsion important for axon guidance and neuronal pathfinding (Nagaraj et al., 2015). Additionally, a recent study of exome sequencing of 1213 CHD parent-offspring trios identified a high prevalence of de novo mutations in genes that important for both heart and brain development (Homsy et al., 2015). Further research will be needed to investigate this possibility in more detail.

Regarding the macrostructural alterations in topology, our previous study involving older adolescents (ages 13-16) with transposition of the great arteries (TGA) supports a link between hierarchical structural topology and later neurodevelopmental outcome (Panigrahy et al., 2015), as changes in small-worldness and modularity compared to normal referents mediated neurocognitive performance across a variety of domains, including learning and memory, executive function, and visual-spatial. Peri-operative factors were also significant, as duration of intraoperative cooling during the arterial switch operation (for surgical correction of TGA) exerted a strong neuroprotective effect, enhancing neurocognitive functioning across all domains assessed (mediated by small-worldness and modularity),

while a longer hospital stay exerted deleterious effects (mediated by small-worldness and modularity).

Methodological Considerations

In order to best delineate structural network topology differences in neonatal CHD patients, we applied innovative post-processing and statistical methodology that assisted with characterization of both microstructural and macrostructural alterations. For the graph analyses, both unweighted (binarized adjacency matrices) and weighted (# tracts or average FA) graphs were used, as separate information is available from each. The sensitivity of the various graph analyses (adjacency/# tracts/average FA) lies on a continuum with the average FA connectome being more sensitive to microstructural change, as the graph weights are directly related to a DTI microstructural parameter (FA). Adjacency, on the other hand, is the least sensitive to microstructural change as it needs only one streamline to connect between areas, irrespective of the FA values. Thus, the highest degrees of statistical significance for cost/global efficiency were found in the mean FA and # tracts connectomes, consistent with the changes in DTI microstructure and with our secondary analyses relating DTI metrics to network topology parameters. Macrostructural changes may also be separated from microstructural changes seen here via controlling for cost in the analysis, and, consistent with this interpretation, we see higher significance in the adjacency connectome for global efficiency controlling for cost. Higher significance was seen in the # tracts and average FA connectomes for the small-worldness metric controlling for cost, which we interpret as hierarchical fiber reorganization involving changes in relative strength of connections (which adjacency is unable to measure) rather than creation and destruction of connections.

Typically, the absolute FA value is used to find the starting and stopping points for the tractography. Thus, FA differences (known to exist in CHD patients) may artificially affect the topology due to differences in starting and stopping points in the tractography. Thus, an alternative approach was developed based on white matter segmentation. For the voxelwise analysis, a VBA approach (despite its lower sensitivity) was used for the voxelwise analysis in preference to a TBSS approach, since the TBSS approach is more vulnerable to spurious results due to gross morphological differences such as ventriculomegaly often seen in this population.

Limitations

Our study has several limitations. First, we excluded CHD infants with brain injury (stroke and/or punctate white matter injury), and there was a low incidence of postoperative injury compared to other studies. This could reflect the fact that the majority of the studies performed were not clinically indicated, or may be related to the timing of some post-operative scans which were acquired at 2- 3 months postnatal age (an earlier postoperative scan performed 1-2 weeks postoperatively would likely be more sensitive to punctate white matter injury). Since 3D T1 and blood sensitive imaging was acquired in most cases, under detection related to technical factors is felt to be less likely. Our study is limited in that our sample consisted of a cross-sectional heterogeneous group of CHD lesions which have a variety of surgical correction and post-operative courses and included infants that had surgery up to three months of age postnatally (most of these were CHD infants with

Tetralogy of Fallot). In future work, we plan on recruiting larger subgroups of CHD lesions for more detailed analysis of associated network topology changes associated with specific types of CHD lesions and attaining both pre-operative and post-operative scans on the same patients. Our sample size was likely too small in this study to detect differences related to type of lesion. Additionally, while our cross-sectional analyses did show some differences between CHD infants scanned pre-operatively and post-operatively (in the number of tracts connectome), a future longitudinal study will be necessary to precisely delineate effects of operation. Important prenatal, peri-operative and post-operative factors have been shown to influence microstructural measurement in CHD at different ages (Dimitropoulos et al., 2013), which were not addressed in this study. However, in future work, we plan on looking at the relationship between these clinical modifiable and non-modifiable risk factors and structural network topology in neonatal CHD in relation to neurodevelopmental outcomes. Given the difficulty in obtaining reliable and robust fetal brain diffusion tensor imaging, our results suggest that postnatal FA-dependent metabolic wiring cost measurements in CHD neonates could be a useful neuroimaging biomarker to test the efficacy of future fetal interventional therapeutics aimed at reversing the impact of abnormal white matter development in the last trimester including maternal hyperoxygenation, glucose substrates, progesterone or other agents (Frommelt, 2014; Licht, 2015; You et al., 2015).

Finally, the multi-site/platform nature of the study presents some challenges. Multi-site studies have the benefit of increasing sample size and hence power, when the number of potential participants at a single site is limited (as is the case with CHD). However, the possible effect of scanner needs to be rigorously controlled for. Differences in pulse sequence parameters (e.g. length of diffusion encoding gradients, bandwidth, etc.), image SNR, and hardware differences such as gradient slew rates, eddy currents, and shims all will vary across platforms and affect DTI and graph analysis metrics. Indeed, our secondary analyses have demonstrated a significant effect of scanner, especially for metrics such as cost and global efficiency (data not shown). We have controlled for effect of scanner by not only including scanner as a covariate but modeling different between-subject variances dependent on scanner, and shown that these variances are in fact similar. We have also demonstrated from human phantom data a high degree of reliability for graph metrics (nodal/global efficiency) and DTI metrics (FA/AD).

CONCLUSION

We demonstrate cost-dependent network inefficiencies in neonatal CHD pre-operatively and post-operatively compared to controls, related to WM microstructural change. Controlling for cost, we show the presence of increased small-worldness (hierarchical fiber organization) in CHD infants pre-operatively, that persists in the post-operative period compared to controls, suggesting the early presence of brain reorganization. Taken together, these changes may be related to both metabolic derangement secondary to prenatal hypoxic-ischemia/fetal substrate delivery (Limperopoulos et al., 2000; Sun et al., 2015), but also likely genetic factors that are involved in programmed fetal development including important cortical regions (Chen et al., 2012; Fornito et al., 2011; Poldrack and Farah, 2015; Wedeen et al., 2012). These results suggest a connectome analysis will reflect aberrant postnatal fiber density and organization in complex CHD which is relevant for

understanding the basis of cortical reorganization and poor neurodevelopmental outcome. Our methodology also provides a pipeline for quantitation of network topology changes in neonates and infants with microstructural brain dysmaturation at risk for perinatal brain injury

Acknowledgements:

APPENDIX

Node abbreviations

Node abbreviations used in the Figures are given below.

Node	Abbreviation	Node	Abbreviation	Node	Abbreviation
Amygdala_L	AMYG.L	Frontal_Sup_Medial_R	SFGmed.R	Parietal_Sup_L	SPG.L
Amygdala_R	AMYG.R	Frontal_Sup_Orb_L	ORBsup.L	Parietal_Sup_R	SPG.R
Angular_L	ANG.L	Frontal_Sup_Orb_R	ORBsup.R	Postcentral_L	PoCG.L
Angular_R	ANG.R	Frontal_Sup_R	SFGdor.R	Postcentral_R	PoCG.R
Calcarine_L	CAL.L	Fusiform_L	FFG.L	Precentral_L	PreCG.L
Calcarine_R	CAL.R	Fusiform_R	FFG.R	Precentral_R	PreCG.R
Caudate_L	CAU.L	Heschl_L	HES.L	Precuneus_L	PCUN.L
Caudate_R	CAU.R	Heschl_R	HES.R	Precuneus_R	PCUN.R
Cingulum_Ant_L	ACG.L	Hippocampus_L	HIP.L	Putamen_L	PUT.L
Cingulum_Ant_R	ACG.R	Hippocampus_R	HIP.R	Putamen_R	PUT.R
Cingulum_Mid_L	DCG.L	Insula_L	INS.L	Rectus_L	REC.L
Cingulum_Mid_R	DCG.R	Insula_R	INS.R	Rectus_R	REC.R
Cingulum_Post_L	PCG.L	Lingual_L	LING.L	Rolandic_Oper_L	ROL.L
Cingulum_Post_R	PCG.R	Lingual_R	LING.R	Rolandic_Oper_R	ROL.R
Cuneus_L	CUN.L	Occipital_Inf_L	IOG.L	Supp_Motor_Area_L	SMA.L
Cuneus_R	CUN.R	Occipital_Inf_R	IOG.R	Supp_Motor_Area_R	SMA.R
Frontal_Inf_Oper_L	IFGoperc.L	Occipital_Mid_L	MOG.L	SupraMarginal_L	SMG.L
Frontal_Inf_Oper_R	IFGoperc.R	Occipital_Mid_R	MOG.R	SupraMarginal_R	SMG.R
Frontal_Inf_Orb_L	ORBinf.L	Occipital_Sup_L	SOG.L	Temporal_Inf_L	ITG.L
Frontal_Inf_Orb_R	ORBinf.R	Occipital_Sup_R	SOG.R	Temporal_Inf_R	ITG.R
Frontal_Inf_Tri_L	IFGtriang.L	Olfactory_L	OLF.L	Temporal_Mid_L	MTG.L
Frontal_Inf_Tri_R	IFGtriang.R	Olfactory_R	OLF.R	Temporal_Mid_R	MTG.R

Node	Abbreviation	Node	Abbreviation	Node	Abbreviation
Frontal_Med_Orb_L	ORBsupmed.L	Pallidum_L	PAL.L	Temporal_Pole_Mid_L	TPOmid.L
Frontal_Med_Orb_R	ORBsupmed.R	Pallidum_R	PAL.R	Temporal_Pole_Mid_R	TPOmid.R
Frontal_Mid_L	MFG.L	Paracentral_Lobule_L	PCL.L	Temporal_Pole_Sup_L	TPOsup.L
Frontal_Mid_Orb_L	ORBmid.L	Paracentral_Lobule_R	PCL.R	Temporal_Pole_Sup_R	TPOsup.R
Frontal_Mid_Orb_R	ORBmid.R	ParaHippocampal_L	PHG.L	Temporal_Sup_L	STG.L
Frontal_Mid_R	MFG.R	ParaHippocampal_R	PHG.R	Temporal_Sup_R	STG.R
Frontal_Sup_L	SFGdor.L	Parietal_Inf_L	IPL.L	Thalamus_L	THA.L
Frontal_Sup_Medial_L	SFGmed.L	Parietal_Inf_R	IPL.R	Thalamus_R	THA.R

Effect of varying white matter threshold

Attached below are Spearman correlation coefficients between cost and global efficiency obtained at white matter thresholds of 70%, 78% (used for the analyses in the paper), and 86% for the adjacency, # of tracts, and average FA connectomes, showing a very high correlation and thus not a large dependence on the specific white matter threshold used.

COST

Adjacency Connectome

Spearman's R	70%	78%	86%
70%	1.0	0.98	0.95
78%	0.98	1.0	0.97
86%	0.95	0.97	1.0

of Tracts Connectome

Spearman's R	70%	78%	86%
70%	1.0	0.99	0.96
78%	0.99	1.0	0.98
86%	0.96	0.98	1.0

Average FA Connectome

Spearman's R	70%	78%	86%
70%	1.0	0.99	0.97
78%	0.99	1.0	0.99
86%	0.97	0.99	1.0

GLOBAL EFFICIENCY

Adjacency Connectome

Spearman's R	70%	78%	86%
70%	1.0	0.97	0.95
78%	0.97	1.0	0.97
86%	0.95	0.97	1.0

of Tracts Connectome

Spearman's R	70%	78%	86%
70%	1.0	0.99	0.96
78%	0.99	1.0	0.98
86%	0.96	0.98	1.0

Average FA Connectome

Spearman's R	70%	78%	86%
70%	1.0	0.98	0.96
78%	0.98	1.0	0.98
86%	0.96	0.98	1.0

Influence of Scanner

Attached below is an analysis of between-scanner variability based on the same adult subject being scanned on two scanners (Siemens (CHP) and Philips (CHLA)) both for DTI metrics (FA, MD, RD, AD), global graph analysis metrics (cost, global efficiency) and nodal graph metrics (nodal efficiency), compared with inter-subject variability from the infant data (separated out by scanner).

DTI Metrics

For adult phantom, DTI metrics are taken from all voxels with WM probability > 0.78, after spatially coregistering scans between Siemens (CHP) and Philips (CHLA). Correlation coefficients, as well as mean and std. of difference in parameters are computed. For the infant data, the square root of the inter-subject variance (averaged over all voxels) is given for each platform.

Metric	Adult Human Phantom Data (Correlation)	Infant Data (Mean Between-Subject Variability)		
		Siemens (CHP)	Philips (CHLA)	GE (CHP)
FA	0.76	0.0587	0.061	0.078

Metric	Adult Human Phantom Data (Correlation)	Infant Data (Mean Between-Subject Variability)		
		Siemens (CHP)	Philips (CHLA)	GE (CHP)
AD (10^{-3} mm^2/s)	0.79	0.164	0.191	0.199
RD (10^{-3} mm^2/s)	0.57	0.126	0.158	0.164
MD (10^{-3} mm^2/s)	0.526	0.122	0.156	0.160

Nodal Metrics

A similar analysis is performed for nodal efficiency for each of the three connectomes; computations are performed across the 90 nodes in the parcellation atlas.

Connectome	Adult Human Phantom Data (Correlation)	Infant Data (Mean Between-Subject Variability)		
		Siemens (CHP)	Philips (CHLA)	GE (CHP)
Adjacency	0.82	0.069	0.078	0.074
# of Tracts	0.91	0.86	0.82	0.73
Average FA	0.81	0.022	0.023	0.029

Global Metrics

Results are given for global metrics (cost/global efficiency); for the adult human phantom data correlation coefficients for cost and global efficiency are estimated from bootstrap resampling (1000 samples with replacement) the graph weights and nodal efficiency, respectively.

| Connectome	Metric	Adult Human Phantom Data (Correlation)	Infant Data (Between-Subject Variability)		
			Siemens (CHP)	Philips (CHLA)	GE (CHP)
Adjacency	Cost	0.71	0.0085	0.0081	0.0085
# of Tracts	Cost	0.84	0.091	0.0850	0.080
Average FA	Cost	0.66	0.0028	0.0023	0.0041
Adjacency	Global Efficiency	0.81	0.027	0.036	0.034
# of Tracts	Global Efficiency	0.91	0.44	0.45	0.41
Average FA	Global Efficiency	0.81	0.114	0.117	0.178

References

Alcauter S, Lin W, Smith JK, Gilmore JH, Gao W. (2015): Consistent anterior-posterior segregation of the insula during the first 2 years of life. Cereb Cortex 25(5):1176–1187. [PubMed: 24248433]

Ball G, Aljabar P, Zebari S, Tusor N, Arichi T, Merchant N, Robinson EC, Ogundipe E, Rueckert D, Edwards AD. (2014): Rich-club organization of the newborn human brain. Proceedings of the National Academy of Sciences 111(20):7456–7461.

Batalle D, Eixarch E, Figueras F, Muñoz-Moreno E, Bargallo N, Illa M, Acosta-Rojas R, Amat-Roldan I, Gratacos E. (2012): Altered small-world topology of structural brain networks in infants with intrauterine growth restriction and its association with later neurodevelopmental outcome. Neuroimage 60(2):1352–1366. [PubMed: 22281673]

Beca J, Gunn JK, Coleman L, Hope A, Reed PW, Hunt RW, Finucane K, Brizard C, Dance B, Shekerdemian LS. (2013): New white matter brain injury after infant heart surgery is associated with diagnostic group and the use of circulatory arrest. Circulation 127(9):971–9. [PubMed: 23371931]

Bellinger DC, Watson CG, Rivkin MJ, Robertson RL, Roberts AE, Stopp C, Dunbar-Masterson C, Bernson D, DeMaso DR, Wypij D. (2015): Neuropsychological Status and Structural Brain Imaging in Adolescents With Single Ventricle Who Underwent the Fontan Procedure. J Am Heart Assoc 4(12):e002302. [PubMed: 26667085]

Bellinger DC, Wypij D, Rivkin MJ, DeMaso DR, Robertson RL, Jr., Dunbar-Masterson C, Rappaport LA, Wernovsky G, Jonas RA, Newburger JW. (2011): Adolescents with d-transposition of the great arteries corrected with the arterial switch procedure: neuropsychological assessment and structural brain imaging. Circulation 124(12):1361–9. [PubMed: 21875911]

Benjamini Y, Hochberg Y. (2000): On the Adaptive Control of the False Discovery Rate in Multiple Testing with Independent Statistics. Journal of Educational and Behavioral Statistics 25(1):60–83.

Brown CJ, Miller SP, Booth BG, Andrews S, Chau V, Poskitt KJ, Hamarneh G. (2014): Structural network analysis of brain development in young preterm neonates. Neuroimage 101:667–680. [PubMed: 25076107]

Bullmore E, Sporns O. (2009): Complex brain networks: graph theoretical analysis of structural and functional systems. Nat Rev Neurosci 10(3):186–98. [PubMed: 19190637]

Bullmore E, Sporns O. (2012): The economy of brain network organization. Nat Rev Neurosci 13(5): 336–49. [PubMed: 22498897]

Cao M, He Y, Dai Z, Liao X, Jeon T, Ouyang M, Chalak L, Bi Y, Rollins N, Dong Q and others. (2017): Early Development of Functional Network Segregation Revealed by Connectomic Analysis of the Preterm Human Brain. Cereb Cortex 27(3):1949–1963. [PubMed: 26941380]

Chen C-H, Gutierrez E, Thompson W, Panizzon MS, Jernigan TL, Eyler LT, Fennema-Notestine C, Jak AJ, Neale MC, Franz CE. (2012): Hierarchical genetic organization of human cortical surface area. Science 335(6076):1634–1636. [PubMed: 22461613]

Clouchoux C, du Plessis A, Bouyssi-Kobar M, Tworetzky W, McElhinney D, Brown D, Gholipour A, Kudelski D, Warfield S, McCarter R. (2013): Delayed cortical development in fetuses with complex congenital heart disease. Cereb Cortex 23(12):2932–2943. [PubMed: 22977063]

Collin G, van den Heuvel MP. (2013): The Ontogeny of the Human Connectome Development and Dynamic Changes of Brain Connectivity Across the Life Span. The Neuroscientist 19(6):616–628 %@ 1073-8584. [PubMed: 24047610]

Di Martino A, Fair DA, Kelly C, Satterthwaite TD, Castellanos FX, Thomason ME, Craddock RC, Luna B, Leventhal BL, Zuo X-N. (2014): Unraveling the miswired connectome: a developmental perspective. Neuron 83(6):1335–1353 %@ 0896-6273. [PubMed: 25233316]

Dimitropoulos A, McQuillen PS, Sethi V, Moosa A, Chau V, Xu D, Brant R, Azakie A, Campbell A, Barkovich AJ. (2013): Brain injury and development in newborns with critical congenital heart disease. Neurology 81(3):241–248. [PubMed: 23771484]

Fling BW, Kwak Y, Peltier SJ, Seidler RD. (2012): Differential relationships between transcallosal structural and functional connectivity in young and older adults. Neurobiol Aging 33(10):2521–2526. [PubMed: 22177217]

Fling BW, Peltier SJ, Bo J, Welsh RC, Seidler RD. (2011): Age differences in interhemispheric interactions: callosal structure, physiological function, and behavior. Frontiers in neuroscience 5.

Fornito A, Zalesky A, Bassett DS, Meunier D, Ellison-Wright I, Yücel M, Wood SJ, Shaw K, O'Connor J, Nertney D. (2011): Genetic influences on cost-efficient organization of human cortical functional networks. The Journal of Neuroscience 31(9):3261–3270. [PubMed: 21368038]

Frommelt MA. (2014): Challenges and Controversies in Fetal Diagnosis and Treatment: Hypoplastic Left Heart Syndrome. Clin Perinatol 41(4):787–798. [PubMed: 25459774]

Gao W, Alcauter S, Smith JK, Gilmore JH, Lin W. (2014): Development of human brain cortical network architecture during infancy. Brain Structure and Function 220(2):1173–1186. [PubMed: 24469153]

Gao W, Gilmore JH, Giovanello KS, Smith JK, Shen D, Zhu H, Lin W. (2011): Temporal and spatial evolution of brain network topology during the first two years of life. PLoS One 6(9):e25278. [PubMed: 21966479]

Gao W, Gilmore JH, Shen D, Smith JK, Zhu H, Lin W. (2013): The synchronization within and interaction between the default and dorsal attention networks in early infancy. Cereb Cortex 23(3): 594–603. [PubMed: 22368080]

Gaynor JW. (2014): The encephalopathy of congenital heart disease. J Thorac Cardiovasc Surg 148(5): 1790–1791. [PubMed: 25444179]

Gaynor JW, Stopp C, Wypij D, Andropoulos DB, Atallah J, Atz AM, Beca J, Donofrio MT, Duncan K, Ghanayem NS. (2015): Neurodevelopmental outcomes after cardiac surgery in infancy. Pediatrics 135(5):816–825. [PubMed: 25917996]

Hagmann P, Grant PE, Fair DA. (2012): MR connectomics: a conceptual framework for studying the developing brain. Front Syst Neurosci 6.

Hoffman GM, Brosig CL, Bear LM, Tweddell JS, Mussatto KA. (2015): Effect of Intercurrent Operation and Cerebral Oxygenation on Developmental Trajectory in Congenital Heart Disease. The Annals of thoracic surgery.

Homsy J, Zaidi S, Shen Y, Ware JS, Samocha KE, Karczewski KJ, DePalma SR, McKean D, Wakimoto H, Gorham J. (2015): De novo mutations in congenital heart disease with neurodevelopmental and other congenital anomalies. Science 350(6265):1262–1266. [PubMed: 26785492]

Huang H, Shu N, Mishra V, Jeon T, Chalak L, Wang ZJ, Rollins N, Gong G, Cheng H, Peng Y and others. (2015): Development of human brain structural networks through infancy and childhood. Cereb Cortex 25(5):1389–404. [PubMed: 24335033]

Langan J, Peltier SJ, Bo J, Fling BW, Welsh RC, Seidler RD. (2010): Functional implications of age differences in motor system connectivity. Front Syst Neurosci 4.

Ledberg A, Akerman S, Roland PE. (1998): Estimation of the probabilities of 3D clusters in functional brain images. Neuroimage 8(2):113–28. [PubMed: 9740755]

Li Y, Yin S, Fang J, Hua Y, Wang C, Mu D, Zhou K. (2014): Adverse neurological performance with critical congenital heart diseases mainly from prenatal injury not cardiac surgery: current evidence based on a meta-analysis of functional magnetic resonance imaging. Ultrasound in Obstetrics & Gynecology.

Licht DJ. (2015): The Path Forward is to Look Backward in Time-Fetal Physiology: The New Frontier in Managing Infants with Congenital Heart Defects. Circulation:CIRCULATIONAHA. 115.016024.

Licht DJ, SD M, R. CR, Gil W, ML M, NS C, ZR A, ST L, William GJ, Arastoo V. (2009): Brain maturation is delayed in infants with complex congenital heart defects. J Thorac Cardiovasc Surg 137(3):529–36; discussion 536–7. [PubMed: 19258059]

Limperopoulos C, Majnemer A, Shevell MI, Rosenblatt B, Rohlicek C, Tchervenkov C. (2000): Neurodevelopmental status of newborns and infants with congenital heart defects before and after open heart surgery. J Pediatr 137(5):638–645. [PubMed: 11060529]

Menon V. (2011): Large-scale brain networks and psychopathology: a unifying triple network model. Trends Cogn Sci 15(10):483–506. [PubMed: 21908230]

Miller SP, McQuillen PS, Hamrick S, Xu D, Glidden DV, Charlton N, Karl T, Azakie A, Ferriero DM, Barkovich AJ. (2007): Abnormal brain development in newborns with congenital heart disease. New England Journal of Medicine 357(19):1928–1938. [PubMed: 17989385]

Mulkey SB, Ou X, Ramakrishnaiah RH, Glasier CM, Swearingen CJ, Melguizo MS, Yap VL, Schmitz ML, Bhutta AT. (2014): White matter injury in newborns with congenital heart disease: a diffusion tensor imaging study. Pediatric Neurology 51(3):377–383. [PubMed: 25160542]

Mussatto KA, Hoffmann R, Hoffman G, Tweddell JS, Bear L, Cao Y, Tanem J, Brosig C. (2015): Risk Factors for Abnormal Developmental Trajectories in Young Children With Congenital Heart Disease. Circulation 132(8):755–761. [PubMed: 26304667]

Nagaraj UD, Evangelou IE, Donofrio MT, Vezina LG, McCarter R, du Plessis AJ, Limperopoulos C. (2015): Impaired Global and Regional Cerebral Perfusion in Newborns with Complex Congenital Heart Disease. J Pediatr 167(5):1018–24. [PubMed: 26384435]

Newburger JW, Sleeper LA, Bellinger DC, Goldberg CS, Tabbutt S, Lu M, Mussatto KA, Williams IA, Gustafson KE, Mital S and others. (2012): Early developmental outcome in children with hypoplastic left heart syndrome and related anomalies: the single ventricle reconstruction trial. Circulation 125(17):2081–91. [PubMed: 22456475]

Ortinau C, Beca J, Lambeth J, Ferdman B, Alexopoulos D, Shimony JS, Wallendorf M, Neil J, Inder T. (2012a): Regional alterations in cerebral growth exist preoperatively in infants with congenital heart disease. J Thorac Cardiovasc Surg 143(6):1264–70. [PubMed: 22143100]

Ortinau C, Dimitrios A, and DD. (2013): Cortical folding is altered before surgery in infants with congenital heart disease. J Pediatr 163(5):1507–10. [PubMed: 23988135]

Ortinau C, Inder T, Lambeth J, Wallendorf M, Finucane K, Beca J. (2012b): Congenital heart disease affects cerebral size but not brain growth. Pediatric Cardiology 33(7):1138–46. [PubMed: 22450354]

Owen M, Shevell M, Donofrio M, Majnemer A, McCarter R, Vezina G, Bouyssi-Kobar M, Evangelou I, Freeman D, Weisenfeld N and others. (2014): Brain volume and neurobehavior in newborns with complex congenital heart defects. J Pediatr 164(5):1121–1127 e1. [PubMed: 24367983]

Panigrahy A, Schmithorst VJ, Wisnowski JL, Watson CG, Bellinger DC, Newburger JW, Rivkin MJ. (2015): Relationship of white matter network topology and cognitive outcome in adolescents with d-transposition of the great arteries. NeuroImage: clinical 7:438–448. [PubMed: 25685710]

Paquette LB, WJ L, C R, PJ D, and DJA. (2013): Abnormal cerebral microstructure in premature neonates with congenital heart disease. AJNR Am J Neuroradiol 34(10):2026–33. [PubMed: 23703146]

Partridge SC, Vigneron DB, Charlton NN, Berman JI, Henry RG, Mukherjee P, McQuillen PS, Karl TR, Barkovich AJ, Miller SP. (2006): Pyramidal tract maturation after brain injury in newborns with heart disease. Ann Neurol 59(4):640–651. [PubMed: 16450369]

Poldrack RA, Farah MJ. (2015): Progress and challenges in probing the human brain. Nature 526(7573):371–379. [PubMed: 26469048]

Scheinost D, Kwon SH, Shen X, Lacadie C, Schneider KC, Dai F, Ment LR, Constable RT. (2015): Preterm birth alters neonatal, functional rich club organization. Brain Structure and Function:1–12. [PubMed: 24248427]

Schmithorst VJ, Wisnowski J, Panigrahy A. 2013 Robustness of TBSS and VBM-like Voxelwise DTI Analyses. Organization for Human Brain Mapping 19th Annual Meeting Seattle, WA.

Shi F, Yap PT, Wu G, Jia H, Gilmore JH, Lin W, Shen D. (2011): Infant brain atlases from neonates to 1-and 2-year-olds. PLoS One 6(4):e18746. [PubMed: 21533194]

Smith SM, Jenkinson M, Johansen-Berg H, Rueckert D, Nichols TE, Mackay CE, Watkins KE, Ciccarelli O, Cader MZ, Matthews PM and others. (2006): Tract-based spatial statistics: voxelwise analysis of multi-subject diffusion data. Neuroimage 31(4):1487–505. [PubMed: 16624579]

Song L, Mishra V, Ouyang M, Peng Q, Slinger M, Liu S, Huang H. (2017): Human Fetal Brain Connectome: Structural Network Development from Middle Fetal Stage to Birth. Front Neurosci 11:561. [PubMed: 29081731]

Sun L, Macgowan CK, Sled JG, Yoo S-J, Manlhiot C, Porayette P, Grosse-Wortmann L, Jaeggi E, McCrindle BW, Hickey E. (2015): Reduced Fetal Cerebral Oxygen Consumption Is Associated With Smaller Brain Size in Fetuses With Congenital Heart Disease. Circulation:CIRCULATIONAHA. 114.013051.

Thomason ME, Brown JA, Dassanayake MT, Shastri R, Marusak HA, Hernandez-Andrade E, Yeo L, Mody S, Berman S, Hassan SS. (2014): Intrinsic functional brain architecture derived from graph theoretical analysis in the human fetus. PLoS One 9(5):e94423. [PubMed: 24788455]

Thomason ME, Grove LE, Lozon TA, Vila AM, Ye Y, Nye MJ, Manning JH, Pappas A, Hernandez-Andrade E, Yeo L. (2015): Age-related increases in long-range connectivity in fetal functional neural connectivity networks in utero. Developmental cognitive neuroscience 11:96–104. [PubMed: 25284273]

van den Heuvel MP, Kahn RS, Goñi J, Sporns O. (2012): High-cost, high-capacity backbone for global brain communication. Proceedings of the National Academy of Sciences 109(28):11372–11377.

van den Heuvel MP, Kersbergen KJ, de Reus MA, Keunen K, Kahn RS, Groenendaal F, de Vries LS, Benders MJ. (2014): The neonatal connectome during preterm brain development. Cereb Cortex:bhu095.

van den Heuvel MP, Sporns O. (2011): Rich-club organization of the human connectome. The Journal of Neuroscience 31(44):15775–15786. [PubMed: 22049421]

Volpe JJ. (2014): Encephalopathy of Congenital Heart Disease- Destructive and Developmental Effects Intertwined. J Pediatr 164(5):962–5. [PubMed: 24529617]

von Rhein M, Buchmann A, Hagmann C, Dave H, Bernet V, Scheer I, Knirsch W, Latal B, Heart, Group BR. (2015): Severe congenital heart defects are associated with global reduction of neonatal brain volumes. J Pediatr 167(6):1259–1263. e1. [PubMed: 26233604]

von Rhein M, Buchmann A, Hagmann C, Huber R, Klaver P, Knirsch W, Latal B. (2014): Brain volumes predict neurodevelopment in adolescents after surgery for congenital heart disease. Brain 137(1):268–276. [PubMed: 24277720]

Watanabe K, Mie M, Junko M, Chiaki T, Kyo N, Naoki Y, Kazuhisa H, Mayumi I, Sayaka W, Keiich H and others. (2009): Impaired neuroanatomic development in infants with congenital heart disease. J Thorac Cardiovasc Surg 137(1):146–53. [PubMed: 19154917]

Watanabe T, Rees G. (2015): Age-associated changes in rich-club organisation in autistic and neurotypical human brains. Sci Rep 5.

Wedeen VJ, Rosene DL, Wang R, Dai G, Mortazavi F, Hagmann P, Kaas JH, Tseng W-YI. (2012): The geometric structure of the brain fiber pathways. Science 335(6076):1628–1634. [PubMed: 22461612]

Yap PT, Fan Y, Chen Y, Gilmore JH, Lin W, Shen D. (2011): Development trends of white matter connectivity in the first years of life. PLoS One 6(9):e24678. [PubMed: 21966364]

You W, Serag A, Evangelou IE, Andescavage N, Limperopoulos C. Robust motion correction and outlier rejection of in vivo functional MR images of the fetal brain and placenta during maternal hyperoxia; 2015 International Society for Optics and Photonics. p 94170O–94170O-13.

Zeisel A, Zuk O, Domany E. (2011): FDR Control with Adaptive Procedures and FDR Monotonicity. The Annals of Applied Statistics 5(2A):943–968.

Zuo X-N, Ehmke R, Mennes M, Imperati D, Castellanos FX, Sporns O, Milham MP. (2012): Network centrality in the human functional connectome. Cereb Cortex 22(8):1862–1875. [PubMed: 21968567]
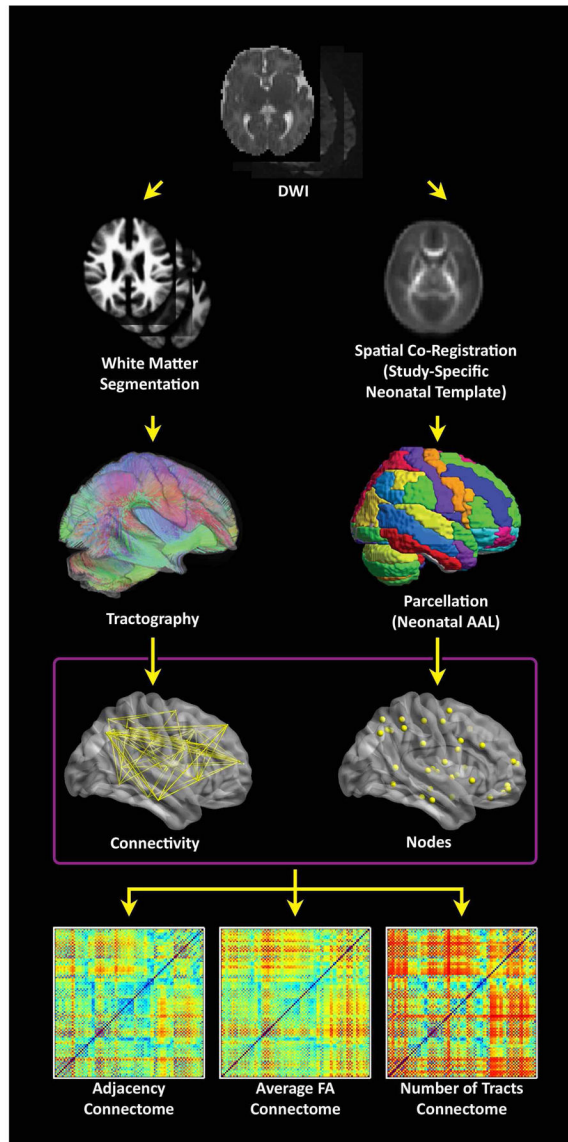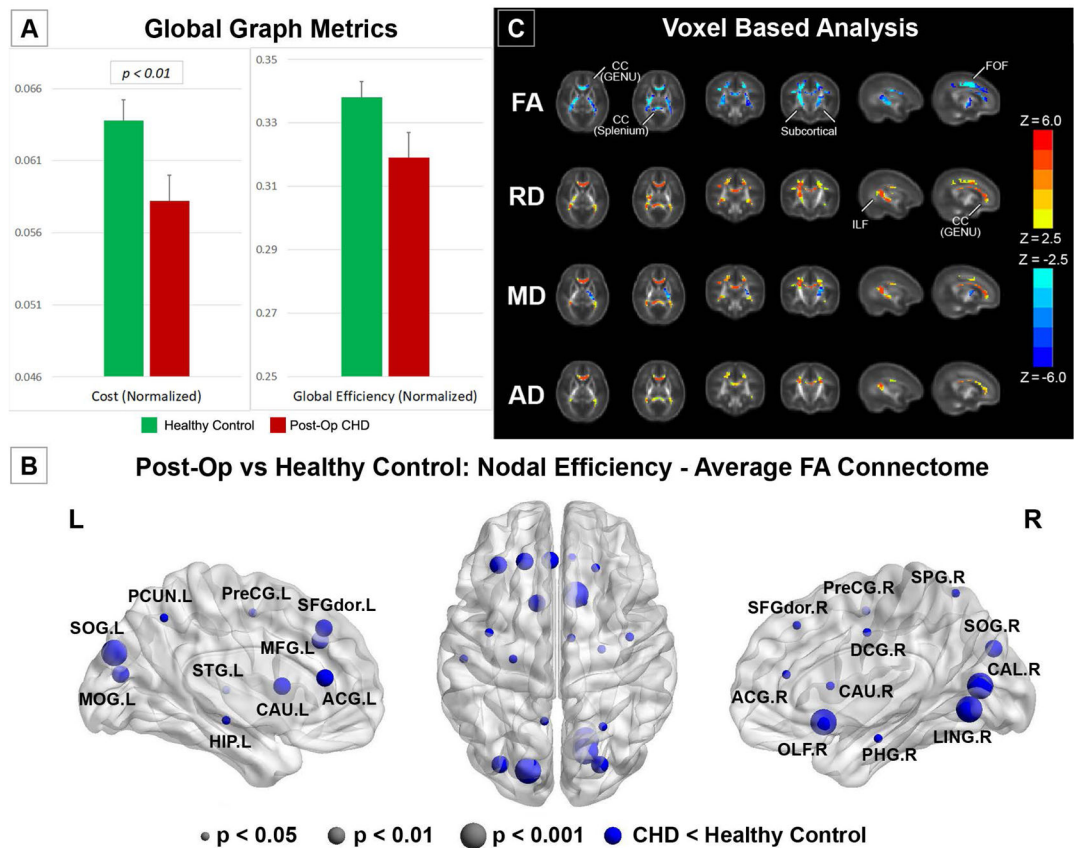
Figure 1.
Flowchart depicting the data processing stream. (Right stream) The λ_1 images are spatially coregistered to a neonatal T2-weighted template (step not shown) and FA images are transformed into standard space using those transformations in order to construct a study-specific FA neonatal template. The template is back-transformed into native space, along with the neonatal parcellation atlas in order to define gray matter regions in native space. (Left stream) A white matter segmentation is performed in SPM8 using the FA images and neonatal GM, WM, and CSF templates. Tractography is then performed starting from each white matter voxel, which avoids the use of a strict FA threshold. (Bottom) Connectomes are computed using either: adjacency (the matrix has 0 or 1 depending on whether there is at least one streamline connecting two regions), average FA (across all streamlines connecting two regions), or the total # of streamlines connecting two regions.
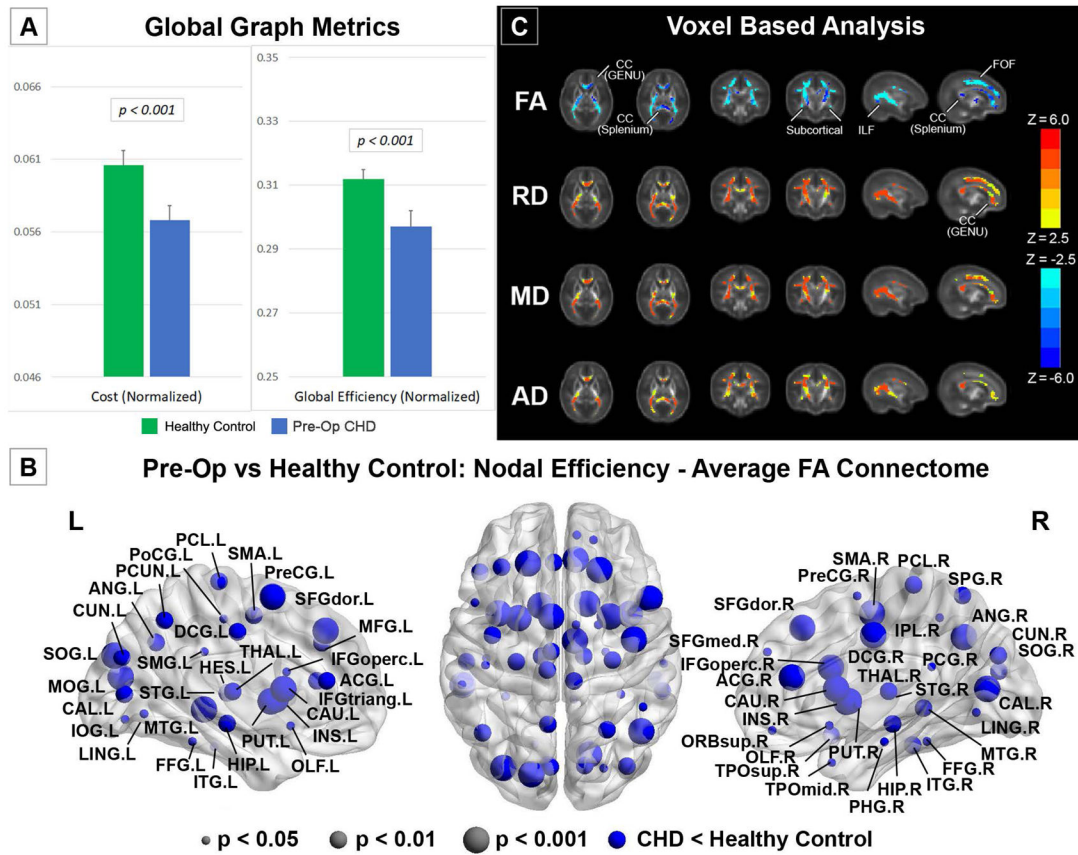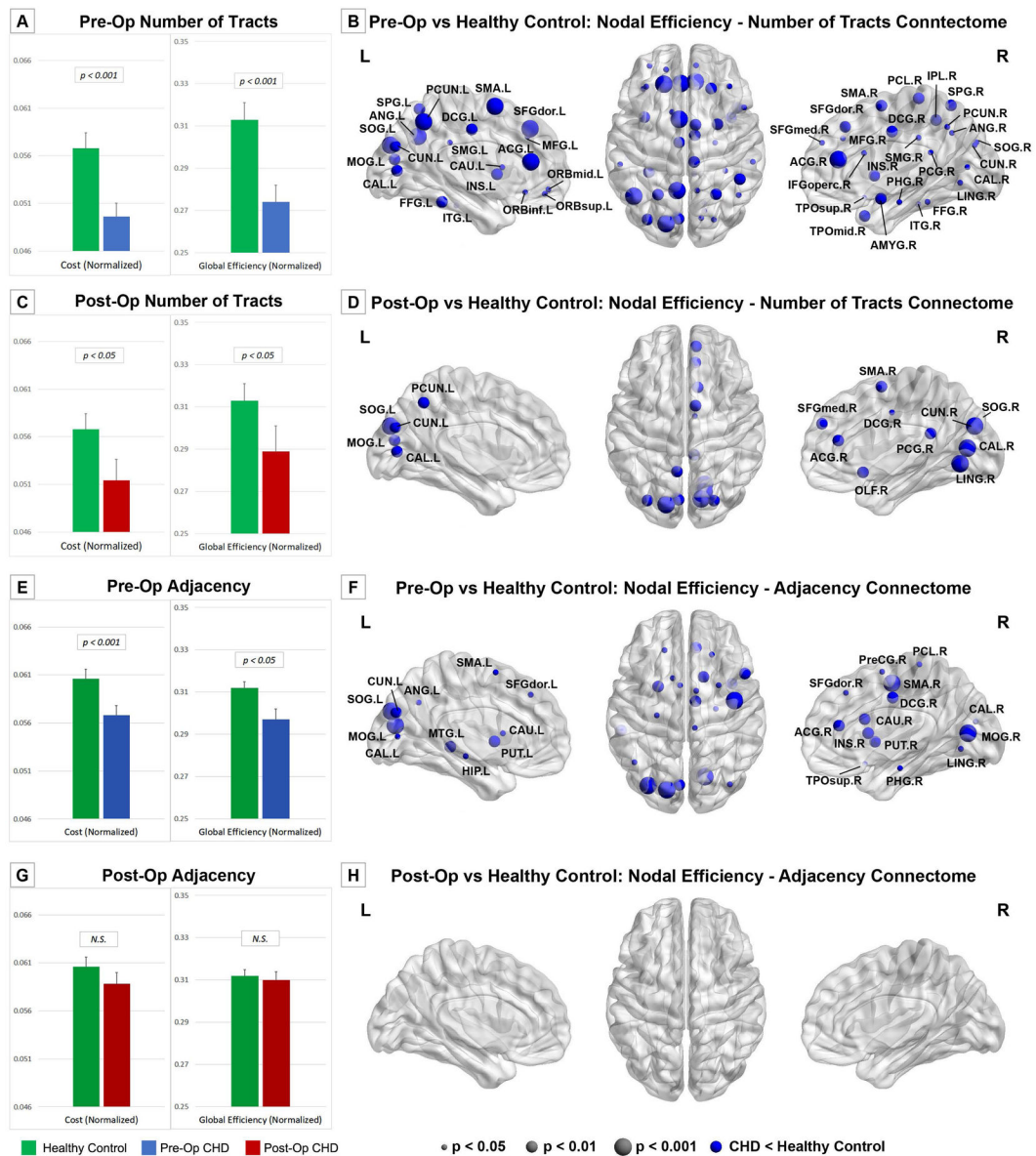
Figure 2.
Comparison between CHD neonates <u>pre-operatively</u> vs. normal healthy controls (average FA connectome): (A) comparison of network cost and global efficiency (values normalized to unity average graph weight); (B) Comparison of nodal efficiency (all regions significant at FDR-corrected q < 0.05); (C) comparison of DTI metrics FA, RD, MD, and AD (hot colors = CHD > controls, cold colors = CHD < controls, all regions significant at FWE-corrected p < 0.05).
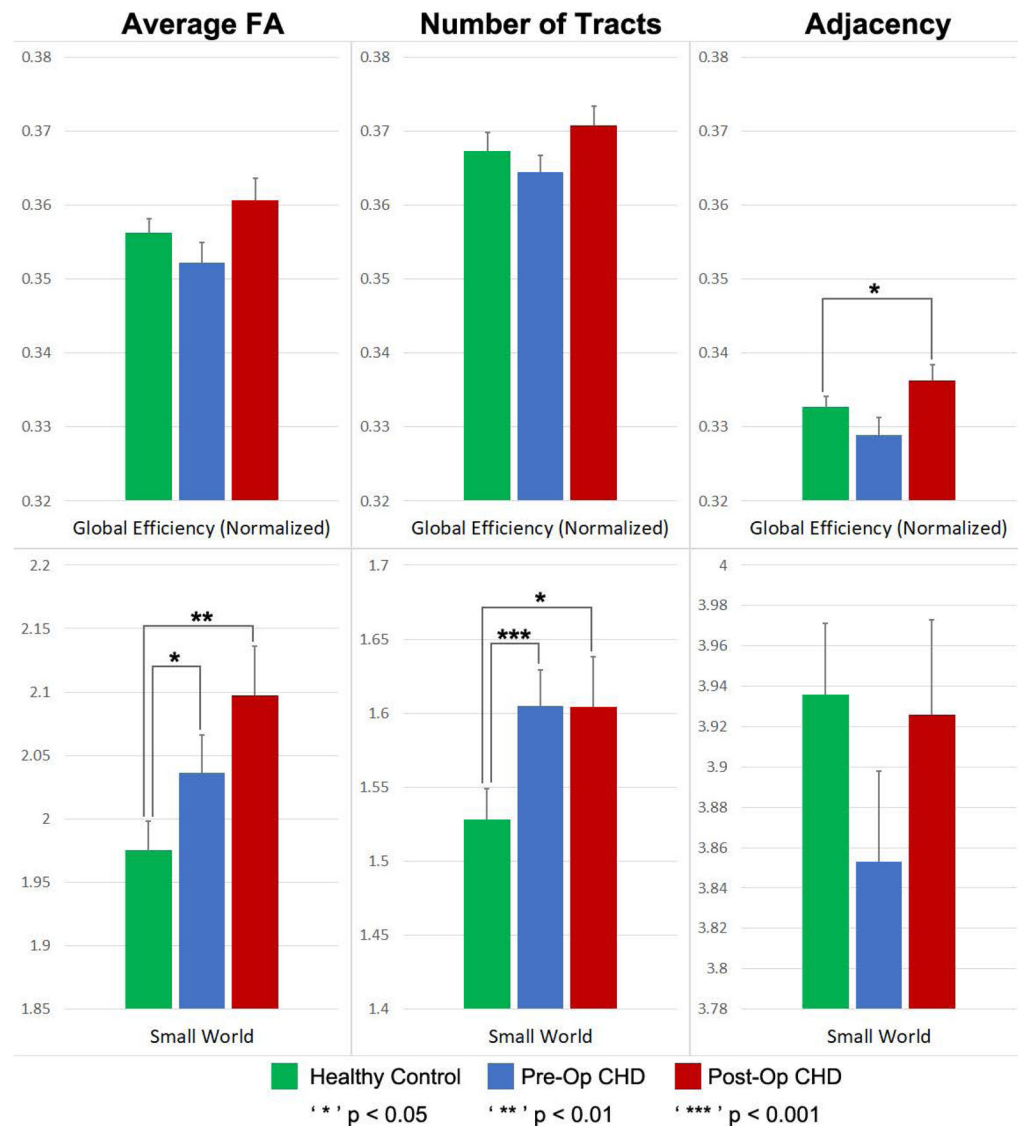
Figure 3.
Comparison between CHD neonates <u>post-operatively</u> vs. normal healthy controls (average FA connectome): (A) comparison of network cost and global efficiency (values normalized to unity average graph weight); (B) Comparison of nodal efficiency (all regions significant at FDR-corrected q < 0.05); (C) comparison of DTI metrics FA, RD, MD, and AD (hot colors = CHD > controls, cold colors = CHD < controls, all regions significant at FWE-corrected p < 0.05).
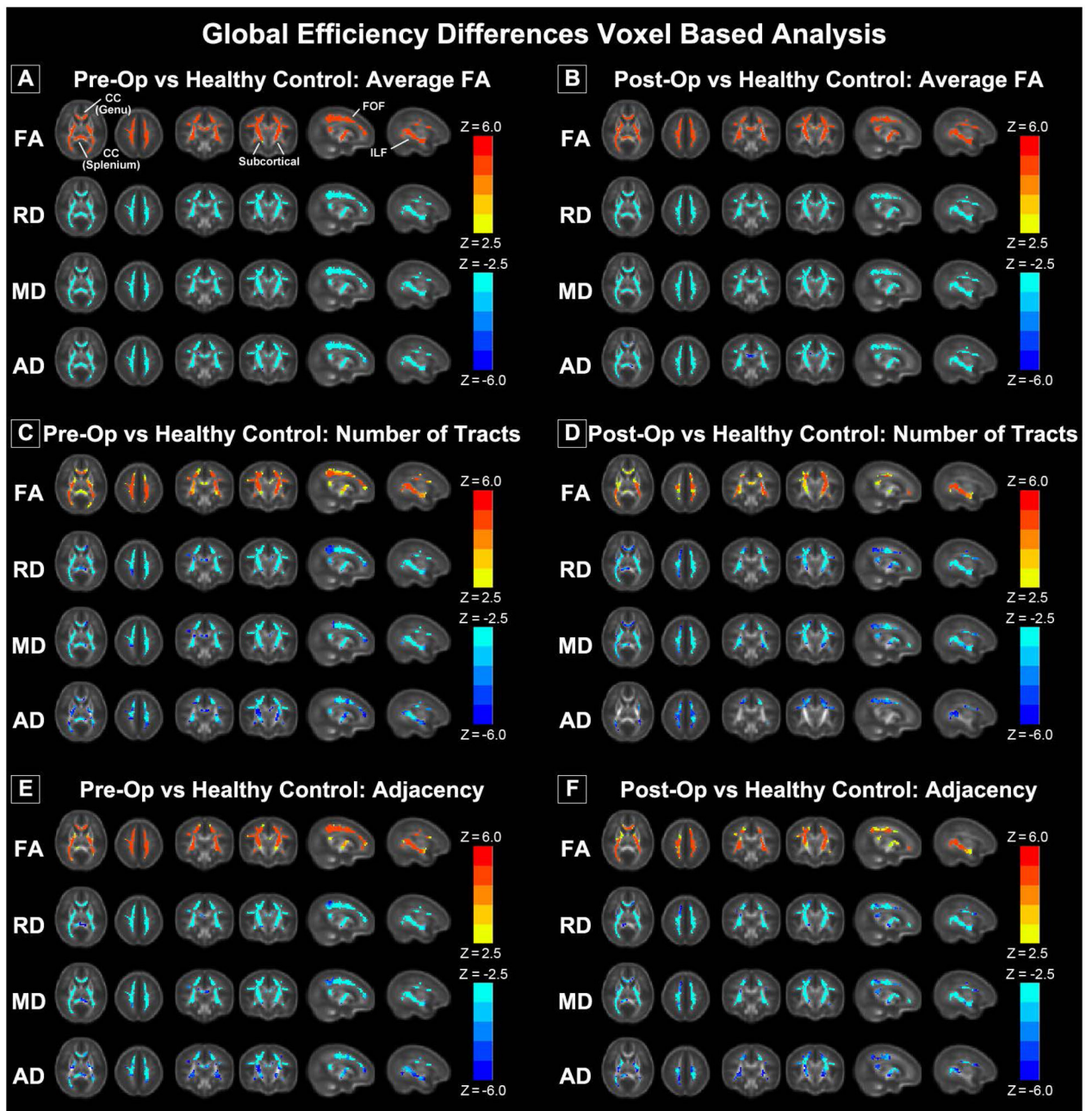
Figure 4.
Comparisons between CHD neonates pre- and post-operatively vs. normal healthy controls: comparison of network cost and global efficiency (values normalized to unity average graph weight) for # tracts connectome (A, C) and adjacency connectome (E, G); Comparison of nodal efficiency (all regions significant at FDR-corrected q < 0.05) for # tracts connectome (B, D) and adjacency connectome (F, H).

Comparison of Global Graph Metrics between Patients with CHD and Healthy Controls (Cost Controlled)

Figure 5.
Comparison of global metrics (global efficiency, small-worldness) between CHD neonates pre-operatively, CHD neonates post-operatively, and normal healthy controls, <u>controlling for network cost</u>. Efficiency normalized to unity average graph weight.

Figure 6.
Correlation of DTI metrics (FA, RD, MD, AD) with global efficiency for pre-operative CHD
(A, C, E) and post-operative CHD (B, D, F) for average FA connectome (A, B), # of tracts
connectome (C, D) and adjacency connectome (E, F). (Hot colors = positive correlation,
cold colors = negative correlation, all regions significant at FWE-corrected p < 0.05).

Table 1.

Demographic characteristics for normal referents, participants with CHD scanned preoperatively, and participants with CHD scanned postoperatively.

	Controls	Pre-operative CHD	Post-operative CHD
N	91 (37 M, 54 F)	61 (37 M, 24 F)	50 (31 M, 19 F)
PCA at Birth (wks)	38.9 +/− 1.06	39.1 +/− 1.02	39.0 +/− 1.08
PCA at Scan (wks)	42.7 +/− 5.14	42.5 +/− 3.69	42.7 +/− 4.66

Table 2.

Heart Lesion Subtype for participants with CHD scanned pre-operatively and participants with CHD scanned post-operatively.

	Pre-operative	Post-operative
N	61	50
Single-Ventricle	28	23
Arch Obstruction	26	21
Transposition Great Arteries	15	12
Cyanotic	54	49
Conotruncal	38	34
Heterotaxy	6	5

Table 3.

p-values for comparison of global graph metrics between patients with CHD scanned pre-operatively vs. normal referents (top), patients with CHD scanned post-operatively vs. normal referents (bottom). (Red font = greater value in CHD scanned pre-operatively; blue font = smaller value in CHD scanned pre-operatively.)

	Adjacency	# T racts	Average FA
CHD scanned pre-operatively vs. normal referents			
Cost	**<.001**	**<.001**	**<.001**
Global Efficiency	**<.05**	**<.001**	**<.001**
Transitivity	N.S.	N.S.	N.S.
Modularity	N.S.	N.S.	N.S.
Small-Worldness	N.S.	N.S.	N.S.
CHD scanned post-operatively vs. normal referents			
Cost	N.S.	**<.05**	**<.01**
Global Efficiency	N.S.	**<.05**	N.S.
Transitivity	**<.05**	N.S.	**<.05**
Modularity	N.S.	N.S.	N.S.
Small-Worldness	N.S.	N.S.	N.S.

Table 4.

p-values for comparison of global graph metrics between patients with CHD scanned pre-operatively vs. normal referents (top), patients with CHD scanned post-operatively vs. normal referents (bottom), controlling for network cost. (Red font = greater value in CHD scanned pre-operatively; blue font = smaller value in CHD scanned pre-operatively.)

	Adjacency	# T racts	Average FA
CHD scanned pre-operatively vs. normal referents			
Global Efficiency	N.S.	N.S.	N.S.
Transitivity	N.S.	N.S.	N.S.
Modularity	N.S.	N.S.	N.S.
Small-Worldness	N.S.	**<.001**	**<.05**
CHD scanned post-operatively vs. normal referents			
Global Efficiency	**<.05**	N.S.	N.S.
Transitivity	N.S.	N.S.	N.S.
Modularity	N.S.	N.S.	N.S.
Small-Worldness	N.S.	**<.05**	**<.01**